Surface plasmon polariton propagation in organic nanofiber based plasmonic waveguides

Till Leißner,[1,*] Christoph Lemke,[1] Stephan Jauernik,[1] Mathias Müller,[1] Jacek Fiutowski,[2] Luciana Tavares,[2] Kasper Thilsing-Hansen,[2] Jakob Kjelstrup-Hansen,[2] Olaf Magnussen,[1] Horst-Günter Rubahn,[2] and Michael Bauer[1]

[1]*University of Kiel, IEAP, Leibnizstr. 19, 24118 Kiel, Germany*
[2]*University of Southern Denmark, Mads Clausen Institute, NanoSYD, Alsion 2, DK-6400 Sønderborg,Denmark*
[*]*leissner@physik.uni-kiel.de*

http://www.ieap.uni-kiel.de/solid/ag-bauer

Abstract: Plasmonic wave packet propagation is monitored in dielectric-loaded surface plasmon polariton waveguides realized from para-hexaphenylene nanofibers deposited onto a 60 nm thick gold film. Using interferometric time resolved two-photon photoemission electron microscopy we are able to determine phase and group velocity of the surface plasmon polariton (SPP) waveguiding mode (0.967c and 0.85c at $\lambda_{\mathrm{Laser}} = 812\,\mathrm{nm}$) as well as the effective propagation length (39 µm) along the fiber-gold interface. We furthermore observe that the propagation properties of the SPP waveguiding mode are governed by the cross section of the waveguide.

OCIS codes: (240.6680) Surface plasmons; (250.5403) Plasmonics; (320.2250) Femtosecond phenomena; (320.7080) Ultrafast devices; (160.4890) Organic materials; (240.6675) Surface photoemission and photoelectron spectroscopy.

References and links

1. W. L. Barnes, A. Dereux, and T. W. Ebbesen, "Surface plasmon subwavelength optics," Nature **424**, 824–830 (2003).
2. D. K. Gramotnev and S. I. Bozhevolnyi, "Plasmonics beyond the diffraction limit," Nat. Photonics **4**, 83–91 (2010).
3. E. Ozbay, "Plasmonics: merging photonics and electronics at nanoscale dimensions," Science **311**, 189–93 (2006).
4. N. J. Halas, "Plasmonics: an emerging field fostered by Nano Letters," Nano Lett. **10**, 3816–3822 (2010).
5. T. W. Ebbesen, C. Genet, and S. I. Bozhevolnyi, "Surface-plasmon circuitry," Physics Today **61**, 44 (2008).
6. R. F. Oulton, V. J. Sorger, T. Zentgraf, R.-M. Ma, C. Gladden, L. Dai, G. Bartal, and X. Zhang, "Plasmon lasers at deep subwavelength scale," Nature **461**, 629–32 (2009).
7. S. I. Bozhevolnyi, V. S. Volkov, E. Devaux, J.-Y. Laluet, and T. W. Ebbesen, "Channel plasmon subwavelength waveguide components including interferometers and ring resonators," Nature **440**, 508–11 (2006).
8. A. L. Pyayt, B. Wiley, Y. Xia, A. Chen, and L. Dalton, "Integration of photonic and silver nanowire plasmonic waveguides," Nat. Nanotechnol. **3**, 660–5 (2008).
9. A. Krasavin and A. Zayats, "Three-dimensional numerical modeling of photonic integration with dielectric-loaded SPP waveguides," Phys. Rev. B **78**, 045425 (2008).

#182243 - $15.00 USD Received 21 Dec 2012; revised 14 Feb 2013; accepted 14 Feb 2013; published 28 Mar 2013

10. J. Grandidier, S. Massenot, G. des Francs, A. Bouhelier, J.-C. Weeber, L. Markey, A. Dereux, J. Renger, M. González, and R. Quidant, "Dielectric-loaded surface plasmon polariton waveguides: Figures of merit and mode characterization by image and Fourier plane leakage microscopy," Phys. Rev. B **78**, 245419 (2008).
11. N.-N. Feng, M. L. Brongersma, and L. Dal Negro, "Metaldielectric slot-waveguide structures for the propagation of surface plasmon polaritons at 1.55 μm," IEEE J. Quantum. Electron. **43**, 479–485 (2007).
12. J. Gosciniak, T. Holmgaard, and S. I. Bozhevolnyi, "Theoretical analysis of long-range dielectric-loaded surface plasmon polariton waveguides," J. Lightwave Technol. **29**, 1473–1481 (2011).
13. T. Holmgaard and S. Bozhevolnyi, "Theoretical analysis of dielectric-loaded surface plasmon-polariton waveguides," Phys. Rev. B **75**, 245405 (2007).
14. R. M. Briggs, J. Grandidier, S. P. Burgos, E. Feigenbaum, and H. A. Atwater, "Efficient coupling between dielectric-loaded plasmonic and silicon photonic waveguides," Nano Lett. **10**, 4851–4857 (2010).
15. J. Grandidier, G. C. des Francs, L. Markey, A. Bouhelier, S. Massenot, J.-C. Weeber, and A. Dereux, "Dielectric-loaded surface plasmon polariton waveguides on a finite-width metal strip," Appl. Phys. Lett. **96**, 063105 (2010).
16. T. Holmgaard, S. Bozhevolnyi, L. Markey, A. Dereux, A. Krasavin, P. Bolger, and A. Zayats, "Efficient excitation of dielectric-loaded surface plasmon-polariton waveguide modes at telecommunication wavelengths," Phys. Rev. B **78** (2008).
17. T. Holmgaard, Z. Chen, S. I. I. Bozhevolnyi, A. Dereux, N. B. All, and L. Markey, "Dielectric-loaded plasmonic waveguide-ring resonators," Opt. Express **17**, 2968–2975 (2009).
18. K. H. Al-Shamery, H. G. Rubahn, and H. Sitter, eds., *Organic Nanostructures for Next Generation Devices* (Springer-Verlag, 2008).
19. I. P. Radko, J. Fiutowski, L. Tavares, H.-G. Rubahn, and S. I. Bozhevolnyi, "Organic nanofiber-loaded surface plasmon-polariton waveguides," Opt. Express **19**, 15155 (2011).
20. F. Balzer, V. Bordo, A. Simonsen, and H.-G. Rubahn, "Optical waveguiding in individual nanometer-scale organic fibers," Phys. Rev. B **67**, 115408 (2003).
21. F. Quochi, F. Cordella, A. Mura, G. Bongiovanni, F. Balzer, and H.-G. Rubahn, "One-dimensional random lasing in a single organic nanofiber," J. Phys. Chem. B **109**, 21690–3 (2005).
22. F. Quochi, F. Cordella, R. Orru, J. E. Communal, P. Verzeroli, A. Mura, G. Bongiovanni, A. Andreev, H. Sitter, and N. S. Sariciftci, "Random laser action in self-organized para-sexiphenyl nanofibers grown by hot-wall epitaxy," Appl. Phys. Lett. **84**, 4454 (2004).
23. J. Beermann, S. I. Bozhevolnyi, V. G. Bordo, and H.-G. Rubahn, "Two-photon mapping of local molecular orientations in hexaphenyl nanofibers," Opt. Commun. **237**, 423–429 (2004).
24. T. Leißner, K. Thilsing-Hansen, C. Lemke, S. Jauernik, J. Kjelstrup-Hansen, M. Bauer, and H.-G. Rubahn, "Surface plasmon polariton emission prompted by organic nanofibers on thin gold films," Plasmonics **7**, 253–260 (2012).
25. F. Balzer, J. Beermann, S. I. Bozhevolnyi, A. C. Simonsen, and H.-G. Rubahn, "Optically active organic microrings," Nano Lett. **3**, 1311–1314 (2003).
26. M. Schiek, F. Balzer, K. Al-Shamery, A. Lützen, and H.-G. Rubahn, "Light-emitting organic nanoaggregates from functionalized p-quaterphenylenes," Soft Matter **4**, 277 (2008).
27. F.-J. Meyer zu Heringdorf, L. Chelaru, S. Möllenbeck, D. Thien, and M. Horn-von Hoegen, "Femtosecond photoemission microscopy," Surf. Sci. **601**, 4700–4705 (2007).
28. A. Kubo, K. Onda, H. Petek, Z. Sun, Y. S. Jung, and H. K. Kim, "Femtosecond imaging of surface plasmon dynamics in a nanostructured silver film." Nano Lett. **5**, 1123–7 (2005).
29. A. Kubo, N. Pontius, and H. Petek, "Femtosecond microscopy of surface plasmon polariton wave packet evolution at the silver/vacuum interface," Nano Lett. **7**, 470–5 (2007).
30. M. Bauer, C. Wiemann, J. Lange, D. Bayer, M. Rohmer, and M. Aeschlimann, "Phase propagation of localized surface plasmons probed by time-resolved photoemission electron microscopy," Appl. Phys. A: Mater. Sci. Process. **88**, 473–480 (2007).
31. W. Swiech, G. Fecher, C. Ziethen, O. Schmidt, G. Schönhense, K. Grzelakowski, C. M. Schneider, R. Frömter, H. Oepen, and J. Kirschner, "Recent progress in photoemission microscopy with emphasis on chemical and magnetic sensitivity," J. Electron Spectrosc. Relat. Phenom. **84**, 171–188 (1997).
32. M. U. Wehner, M. H. Ulm, and M. Wegener, "Scanning interferometer stabilized by use of Pancharatnam's phase," Opt. Lett. **22**, 1455–1457 (1997).
33. M. Müller, Y. Gonzalez-Garcia, C. Pakula, V. Zaporojtchenko, T. Strunskus, F. Faupel, R. Herges, D. Zargarani, and O. Magnussen, "In situ atomic force microscopy studies of reversible light-induced switching of surface roughness and adhesion in azobenzene-containing PMMA films," Appl. Surf. Sci. **257**, 7719–7726 (2011).
34. F. Balzer and H.-G. Rubahn, "Dipole-assisted self-assembly of light-emitting p-nP needles on mica," Appl. Phys. Lett. **79**, 3860 (2001).
35. L. Tavares, J. Kjelstrup-Hansen, and H.-G. Rubahn, "Efficient roll-on transfer technique for well-aligned organic nanofibers," Small **7**, 2460–2463 (2011).
36. K. Thilsing-Hansen and H.-G. Rubahn, "Storage and transfer of organic nanofibers," European Patent **EP2111655** (2008).
37. T. Tamulevičius, A. Šileikait, S. Tamulevičius, M. Madsen, and H.-G. Rubahn, "Scanning electron microscopy

#182243 - $15.00 USD Received 21 Dec 2012; revised 14 Feb 2013; accepted 14 Feb 2013; published 28 Mar 2013

of semiconducting nanowires at low voltages," Mater Sci-Medzg **15**, 86–90 (2009).
38. H. Petek and S. Ogawa, "Femtosecond time-resolved two-photon photoemission studies of electron dynamics in metals," Prog. Surf. Sci. **56**, 239–310 (1997).
39. L. I. Chelaru and F.-J. Meyer zu Heringdorf, "In situ monitoring of surface plasmons in single-crystalline Ag-nanowires," Surf. Sci. **601**, 4541–4545 (2007).
40. C. Lemke, T. Leißner, S. Jauernik, A. Klick, J. Fiutowski, J. Kjelstrup-Hansen, H.-G. Rubahn, and M. Bauer, "Mapping surface plasmon polariton propagation via counter-propagating light pulses," Opt. Express **20**, 12877 (2012).
41. M. Schiek, A. Lützen, R. Koch, K. Al-Shamery, F. Balzer, R. Frese, and H. G. Rubahn, "Nanofibers from functionalized para-phenylene molecules," Appl. Phys. Lett. **86**, 153107 (2005).

1. Introduction

The confinement of surface plasmon polaritons (SPP) to metal-dielectric interfaces makes this kind of propagating electromagnetic modes an essential ingredient when it comes to the realization of broadband nano-photonic devices [1–3]. This perspective is one of the driving forces for the multitude of current research activities in the field of plasmonics [4–6]. It is therefore of utmost importance to develop nanoscale plasmon-optical elements which can be integrated into a device in a flexible manner and to explore in detail their actual impact on the plasmonic propagation. Waveguides are considered as a vital control unit to be used in future nano-photonic circuits. Different plasmonic waveguiding schemes have been proposed and successfully realized in the recent past. Examples include metallic nanowires and nanogrooves, coupled metallic nanodots [7, 8], or dielectric ridges on top of a metal surface [9–12]. The latter hybrid-configuration is often referred to as dielectric-loaded SPP waveguide (DLSPPW) [13]. Particularly polymethyl-methacrylate (PMMA) has been frequently used for DLSPPWs [14–16] and SPP propagation lengths of several ten micrometers in the telecom wavelength regime (1.55 μm) have been reported [17]. Another promising dielectric component for the realization of DLSPPWs are needlelike para-hexaphenylene (p-6P) nanofibers [18]. Their capability to support plasmonic waveguiding has recently been proven by Radko et al., who observed propagating SPP-modes at a p-6P nanofiber/gold interface via leakage radiation microscopy [19]. This adds to a multitude of other interesting optical properties of p-6P nanofibers. Photonic waveguiding was demonstrated up to wavelengths in the near ultraviolet [20]. Furthermore, p-6P nanofibers exhibit a considerable nonlinear optical second-order susceptibility [21] and also one-dimensional random lasing in individual fibers was reported [21–23]. Finally, it was shown that p-6P nanofibers can be used as efficient and highly localized light-couplers for SPP exaction at metal surfaces [24]. This variety regarding the interaction with electromagnetic waves and a high degree of flexibility in tuning structural and optical properties [25–27] make such phenylene-based nanofibers a very attractive component for the use in nano-photonic circuits. This paper reports on the quantitative characterization of plasmonic waveguiding at the interface between individual p-6P nanofibers and a gold substrate. We particularly address peculiarities of SPP propagation that are governed by the 1-dimensional geometrical constraints in combination with the dielectric response of the nanofiber material. For the experiment sub 20-femtosecond SPP wave packets are injected into the waveguide via light coupling and the consequent propagation is probed in a highly local manner by static and interferometric time-resolved photoemission electron microscopy (PEEM) [27–30]. The structural characterization of the addressed fibers by scanning force microscopy (AFM) complements these experiments and allows for a direct correlation of fiber geometry and SPP propagation.

2. Experimental

For static and interferometric time-resolved PEEM experiments we used a photoemission electron microscope with integrated sample stage (IS PEEM, Focus GmbH) [31] mounted in an ul-

#182243 - $15.00 USD Received 21 Dec 2012; revised 14 Feb 2013; accepted 14 Feb 2013; published 28 Mar 2013

trahigh vacuum (UHV) μ-metal chamber (base pressure $1 \cdot 10^{-10}$ mbar) and providing a lateral resolution of better than 40 nm. The samples were excited at an angle of incidence of 65° towards the sample surface normal with ultrashort laser pulses of 18 fs duration at a central wavelength of 812 nm and the plasmonic response was probed via two-photon photoemission [29]. Spectral and temporal pulse characterization was performed by linear and second order autocorrelation measurements, respectively. The experimentally determined pulse parameters were used as direct input for the fit procedure to the PEEM data described later in the publication. For the interferometric time-resolved PEEM (ITR-PEEM) measurements we used an actively stabilized Mach-Zehnder interferometer following a design described in detail in reference [32]. A mercury-vapor lamp attached to the UHV-system provides 4.9 eV photon energy and was used for complementary sample characterization in conventional threshold PEEM mode. Further details of the experimental PEEM setup are described in [24]. AFM measurements were conducted with a Veeco Dimension V AFM in tapping mode using a RTESPA Silicon probe [33]. The nanofibers were grown by molecular beam epitaxy on a freshly cleaved and heated muscovite mica substrate [34]. Parallel aligned DLSPPW were prepared by defined transfer of the p-6P nanofibers onto 60 nm thick gold films deposited on silicon substrates. The transfer of the nanofibers from the mica substrate onto the gold films was performed by a roll-on transfer technique [35] and by a stamping transfer technique [36], respectively. Prior to the photoemission measurements, the samples were in-situ covered with a small amount of cesium (coverage $<<$ 1 monolayer) from a well degassed SAES getter source. This treatment is required to lower the work function of the gold surface from a value of about 5.5 eV to below 3 eV to facilitate a two-photon photoemission (2PPE) process with the 812 nm light pulses. AFM and optical microscopy measurements performed after the PEEM experiments show that the structural and optical properties of the nanofibers are not modified by this treatment. However, we find that the observed photoemission contrast is sensitive to the cesium coverage. Low coverages yield a high two-photon photoemission yield from the nanofibers and a low two-photon photoemission yield from the gold film. For higher coverages the contrast becomes reversed and the two-photon PEEM signal is governed by electrons photo-emitted from the gold film. All data shown in this work were recorded in the low coverage regime. This approach turned out to be very helpful for a clear observation of fiber-located SPP modes.

3. Results

Figure 1(a) shows an optical brightfield microscopy image of p-6P nanofibers after the roll-on transfer onto a gold film. Fiber lengths in the range of 30 to 70 μm are observed and the typical fiber-to-fiber distance lies between 10 and 30 μm. Plasmon propagation in DLSPPWs depends critically on fiber width and fiber height [13], information that can be provided from AFM measurements via nanofiber cross-section analysis. Figure 1(b) is an AFM image of an individual p-6P nanofiber of the sample. AFM cross-section data of five different nanofibers are compared in Fig. 1(c). For the fiber width we find a mean value of 525 nm (FWHM), with a small fiber-to-fiber variation of about ±50 nm. In contrast, the differences in fiber height are significant and we observe values ranging between 40 nm and 85 nm, significantly larger than the difference observed for the fibers as-grown on the mica substrate. We ascribe these differences to the rolling procedure applied within the transfer process.

It should be noted that scanning electron microscopy (SEM) measurements of other samples showed a systematic deviation in the nanofiber width by about 15% towards smaller values in comparison to AFM measurements. This could be an indication that the nanofiber width is slightly overestimated in the AFM experiments. However, we also observe that the nanofibers often get structurally modified during SEM scans [37]. In the following no quantitative statement will made that relies on the accurate knowledge of the nanofiber width.

#182243 - $15.00 USD Received 21 Dec 2012; revised 14 Feb 2013; accepted 14 Feb 2013; published 28 Mar 2013

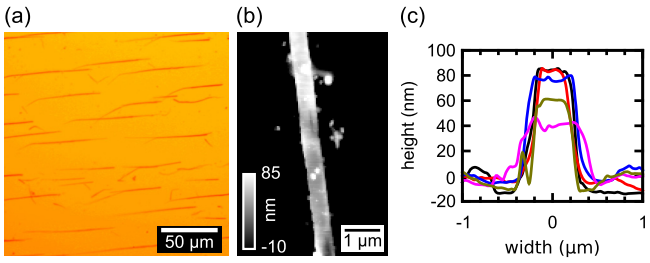

Fig. 1. (a) Optical microscopy image of p-6P nanofibers deposited onto a gold film; the nanofibers (dark shapes) are up to 70 µm in length and their parallel alignment is kept upon deposition; (b) Atomic force microscopy image of a single p-6P nanofiber; (c) cross-section profiles of five different nanofibers of the sample.

The PEEM measurements, which will be presented in the following, were restricted to well separated p-6P nanofibers without any obvious defect sites. Figure 2(a) shows a PEEM image of an individual p-6P nanofiber recorded at illumination with UV light from the mercury vapor lamp ($h\nu = 4.9\,\mathrm{eV}$). SPP modes at this energy are neither supported by the gold-fiber interface nor by the gold-vacuum interface. We therefore can assume that this photoemission image primarily provides information about the fiber geometry. The image shows a rather homogeneous photoemission signal from the fiber and we particularly do not observe any break in the fiber over the entire length of 49 µm. The identical nanofiber is shown in Fig. 2(b), now mapped in the two-photon PEEM mode at excitation with p-polarized laser pulses incident from the left. The image shows clear signatures for the presence of two different plasmonic modes. First, there is a periodically modulated and damped intensity pattern that emerges perpendicular to the nanofiber in both directions into the gold film. In two-photon PEEM, such intensity patterns result from the superposition of an excitation laser field and the polarization field of the (phase-coupled) SPP [29]. The periodic modulation is a beating pattern characteristic for the wave vector mismatch

$$k_{\mathrm{beat}} = k_{\mathrm{SPP}} - k_{\mathrm{Laser}} \tag{1}$$

between SPP and laser pulse. In this specific case, the signal arises from a SPP mode which propagates at the gold-vacuum interface and away from the nanofiber. As has been shown in a preceding work, the local dielectric modulation provided by the nanofiber acts here as an efficient laser-plasmon coupling device [24]. A quantitative analysis of the PEEM intensity pattern shows that SPPs are emitted on both sides of the fiber in forward direction at an angle of about 27° with respect to the fiber orientation.

Secondly, and marked by the red frame in the image, we also observe a periodic modulation in the two-photon photoemission signal along the nanofiber. This signature is assigned to a 1-dimensional SPP waveguiding mode propagating along the gold-nanofiber interface. The 2PPE intensity profile along the nanofiber is shown in black in Fig. 2(c). It is characterized by the periodic modulation and, furthermore, by a decrease in intensity with increasing distance from the left hand fiber end. Overall, we observe similar 2PPE intensity patterns for about 60% of the nanofibers. In all these cases, the pattern emerges from the end of the nanofiber that points towards the incidence direction of the laser pulse.

A Fourier-transformation of the 2PPE intensity profile yields the spectrum shown in Fig. 2(d). The beating pattern signature is the peak in the spectrum at a wave vector $k_{\mathrm{beat}} = (0.160 \pm 0.004)\,\mu\mathrm{m}^{-1}$ corresponding to a periodicity of $(6.25 \pm 0.15)\,\mu\mathrm{m}$. The error includes the broadening of the Fourier spectral distribution (FWHM) and uncertainties in the image calibration (2%). For a laser pulse with a center wavelength of 812 nm and incident onto the sample

#182243 - $15.00 USD Received 21 Dec 2012; revised 14 Feb 2013; accepted 14 Feb 2013; published 28 Mar 2013

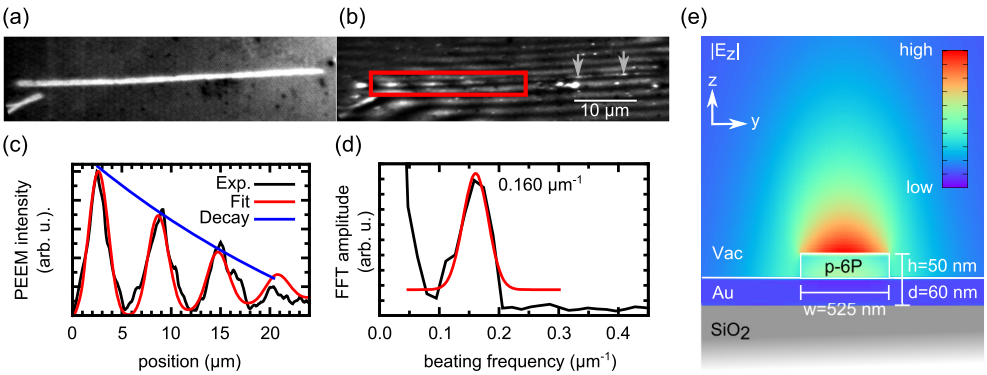

Fig. 2. (a) Threshold PEEM image of a p-6P nanofiber recorded at UV-illumination ($h\nu = 4.9$ eV); (b) same nanofiber imaged at illumination with 18 fs laser pulses at 812 nm central wavelength; the laser light is polarized within the plane of incidence (p-polarized); the red frame marks the periodic DLSPPW signature along the fiber used for the quantitative analysis; (c) experimental two-photon PEEM intensity profile along the p-6P nanofiber (black), corresponding fitted profile (red) and exponential decay of the two-photon PEEM signal (blue); (d) Fourier transformation of the intensity profile yielding a periodicity in the two-photon PEEM signal of 6.25 µm; the red line is a Gaussian fit to the DLSPPW peak; (e) illustration of the electric field distribution (transversal component $|E_z|$ of the fundamental TM_{00} mode) of an SPP waveguiding mode supported by a rectangular p-6P nanofiber on top of a gold surface; the electric field distribution at an excitation wavelength $\lambda_{Laser} = 812$ nm has been calculated using the finite-element method.

at 65°, the wave vector mismatch equation k_{beat} allows us to finally extract the wavelength of the monitored SPP waveguiding mode, $\lambda_{SPP} = 784 \pm 4$ nm [38]. A further quantity that can be provided from this analysis is the effective index of refraction $n_{eff} = \lambda_{Laser}/\lambda_{SPP}$. We find $n_{eff} = 1.036$, a value that agrees very well with data reported for p-6P nanofibers on gold in reference [19].

For illustration Fig. 2(e) depicts the electric field distribution of such a waveguiding mode (transversal component $|E_z|$ of the fundamental TM_{00} mode) as supported by the presence of a nanofiber at the gold surface. Shown are results of a finite-element calculation at an excitation wavelength $\lambda_{Laser} = 812$ nm for a nanofiber with an rectangular cross section of 50 nm × 525 nm on top of a 60 nm thick gold film on SiO_2.

An exponential fit to the 2PPE intensity maxima in 2(c) (blue line) yields a characteristic decay length of the beating pattern of 15 µm. This value can only be considered as the lower limit of the SPP damping length κ which is governed by processes such as ohmic losses, coupling to the radiation field at defects of the nanofiber, or coupling to SPP-modes propagating along the gold-vacuum interface: beside the plasmonic polarization field amplitude the signal probed in a static two-photon PEEM experiment depends, however, also on the group velocity mismatch between laser light and SPP. This quantity determines the effective co-propagation distance of both pulses, and therefore, the effective probing length for SPP propagation. Based on ITR-PEEM data we will provide an accurate value for κ later in this publication.

Figure 3(a) shows static two-photon PEEM images of three further p-6P nanofibers of the same sample. For all fibers we observe a damped periodic beating pattern characteristic for SPP waveguiding. FFT spectra are compared in 3(b). Beating pattern peaks are found at $k_{beat} = (0.165 \pm 0.004)\,\mu m^{-1}$, $(0.166 \pm 0.004)\,\mu m^{-1}$ and $(0.155 \pm 0.004)\,\mu m^{-1}$, respectively yielding SPP wavelength of (780 ± 3) nm, (780 ± 3) nm, and (787 ± 2) nm. These values correspond

#182243 - $15.00 USD Received 21 Dec 2012; revised 14 Feb 2013; accepted 14 Feb 2013; published 28 Mar 2013

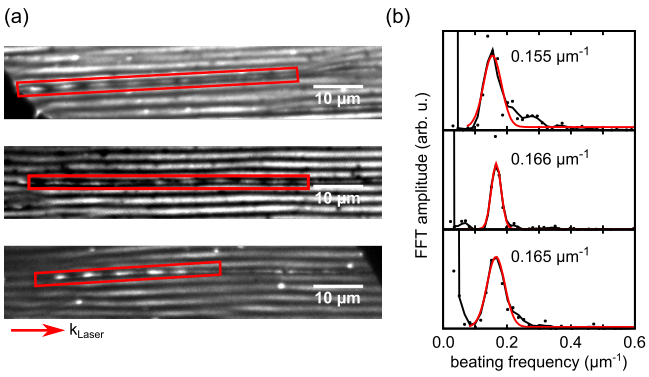

Fig. 3. (a) Three different p-6P nanofibers of the same samples recorded in two-photon PEEM mode; the periodic DLSPPW signatures are marked with red rectangles. (b) Fourier transformation of the intensity profiles along the nanofibers for analysis of the beating pattern periodicity.

to effective indices of refraction of 1.04, 1.04, and 1.03. This result shows that similar fibers, which have been prepared and deposited under identical conditions, support similar SPP modes. Below, we will, however, see that drastic changes of the fiber morphology can substantially modify the waveguiding properties.

ITR-PEEM data enable us to gain further information about the propagation properties of the SPP waveguiding mode. In Fig. 4(a) five selected experimental ITR-PEEM snapshots of the p-6P nanofiber shown in Fig. 2, recorded at different delays within one optical cycle of the excitation laser pulse, are compared. The image series exhibit the typical characteristics for SPP propagation in ITR-PEEM experiments as reported in other works before [24, 29, 39]. The most obvious signature is the split-up of beating pattern maxima for distinct phase delays, starting at a distance of 18 µm from the left hand fiber end (see red arrows). Figure 4(b) shows a delay-intensity profile plot of a complete ITR-PEEM scan, a depiction that provides us quantitative information on SPP phase- and group-velocity. Each horizontal line in the image represents a PEEM intensity profile along the nanofiber measured at a distinct time delay between excitation and probing pulse. For the measurements a delay step width of 0.266 fs was chosen and SPP propagation was probed over a total distance of 45.3 µm. To correct for distortions in the photoemission scans that are not related to the SPP wave packet propagation, in particular some obvious intense spots at large distances (see grey arrows in Fig. 2(b)), a static background profile was subtracted for each delay. Furthermore, the individual delay profiles are intensity normalized, which helps to emphasize the actual wave packet dynamics. The periodic intensity variations in Fig. 4(a) arise from alternating constructive and destructive interference between excitation and probing pulse modulated by the interaction with the propagating plasmon. A first signature in the graph that is directly related to the SPP propagation is a characteristic shift of the interference pattern maxima with the time delay starting at time delays > 20 fs (red dashed line in Fig. 4(b). The slope s of the interference pattern is a measure for the phase velocity of the SPP mode [40].

$$v_{\mathrm{ph,SPP}} = \frac{s \cdot c_{\parallel}}{s + c_{\parallel}}. \tag{2}$$

Here, $c_{\parallel}$ is the component of the vacuum speed of light c projected onto the sample surface plane. A quantitative analysis yields $v_{\mathrm{ph,SPP}} = (0.967 \pm 0.01)c$, a value which is very compatible

#182243 - $15.00 USD Received 21 Dec 2012; revised 14 Feb 2013; accepted 14 Feb 2013; published 28 Mar 2013

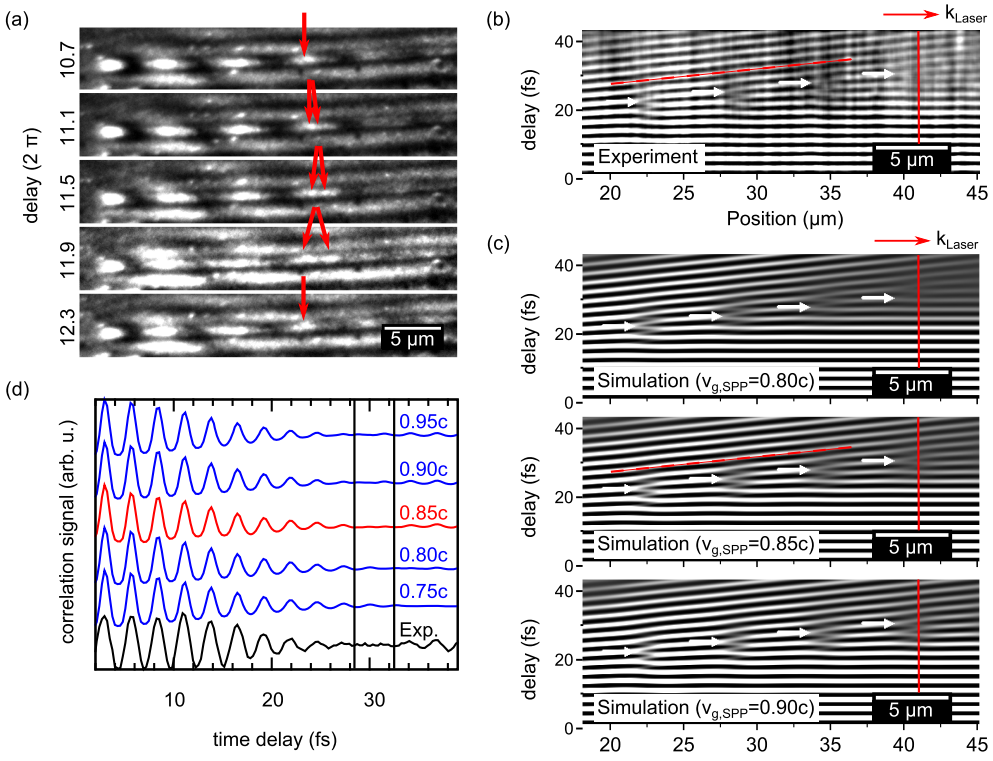

Fig. 4. (a) ITR-PEEM snapshots at five different phase delays within a single oscillation period of the laser field showing the characteristic splitting of the static and the dynamic part of the beating pattern (red arrows); the complete ITR-PEEM movie is provided in the supplemental data (Media 1); (b) ITR-PEEM delay-intensity profile of the p-6P nanofiber shown in Fig. 2; intensity profiles have been corrected for static signal contributions by background subtraction and are normalized to maximum intensity; the slope of the interference pattern indicated by the tilted red dashed line is a indirect measure for the phase velocity of the waveguiding mode; the white arrows indicate the position of splitting signatures characteristic for the group velocity of the waveguiding mode; (c) simulated ITR-PEEM delay-intensity profiles for different group velocities of the SPP wave packet ($0.80\,c$, $0.85\,c$ and $0.90\,c$); the white arrows display the position of the splitting signature as determined in the experiment; (d) simulated ITR-PEEM intensity traces at a fixed position within the fiber (see red lines in Fig. 4(b),(c)) for five different SPP group velocities in comparison to the experimental data (black line).

with the effective index of refraction extracted from the static PEEM data:

$$v_{\mathrm{ph,SPP}} = \frac{\omega_{\mathrm{Laser}}}{k_{\mathrm{SPP}}} = \frac{c}{n_{\mathrm{eff}}} = 0.965c. \tag{3}$$

In a further step the ITR-PEEM results are used to determine the group velocity $v_{\mathrm{g,SPP}}$ at which the SPP wave package is propagating along the gold-nanofiber interface. This quantity can be evaluated from comparison with model simulations with the group velocity $v_{\mathrm{g,SPP}}$ as free adjustment parameter. For the simulations we assumed a Gaussian temporal profile of the excitation laser pulse of 18 fs (FWHM) and a SPP wavelength of 784 nm. The SPP damping constant κ has only very weak influence on the simulated delay-intensity profile patterns, but mainly affects the amplitude, which is not considered here. For convenience the value of κ was set to

#182243 - $15.00 USD Received 21 Dec 2012; revised 14 Feb 2013; accepted 14 Feb 2013; published 28 Mar 2013

60 µm in the simulations.

In the experimental delay-intensity profile plot characteristic nodes are visible where the tilted interference pattern maxima split off from the horizontal interference pattern maxima. These nodes, which are marked in Fig. 4(b) by the white arrows, can be interpreted as a signature of the SPP wave packet envelope separating from the undisturbed interference pattern because of the propagating nature of the plasmon. In fact, the simulations show that the position of the nodes are a critically sensor for the group velocity of the SPP. This is especially the case for the node at 39 µm, since the splitting becomes more evident for larger propagation distances of the SPP wave packet. Figure 4(c) displays simulation results for $v_{g,SPP} = 0.8c$, $v_{g,SPP} = 0.85c$, and $v_{g,SPP} = 0.9c$ for comparison with the experimental data. The position of the nodes as observed in the experiments are indicated by the white arrows. Best agreement with the experiment is found for $v_{g,SPP} = 0.85c$. The sensitivity of the ITR-PEEM data to the SPP group velocity is furthermore highlighted in Fig. 4(d) which shows an experimental intensity-delay trace at a fixed nanofiber position of 40.8 µm (see red line in Fig. 4(b)) in comparison to corresponding simulations calculated for different values of $v_{g,SPP}$. In the graph, the two vertical black lines separate the pure (horizontal) laser interference pattern at the left from the interference pattern affected by the SPP propagation at the right. At the particular fiber position the experimental data do not show any periodic modulation in the photoemission signal amplitude in the interstitial area between the two lines. The comparison with the simulations once again shows that this behavior can be best reproduced for $v_{g,SPP} = 0.85c$.

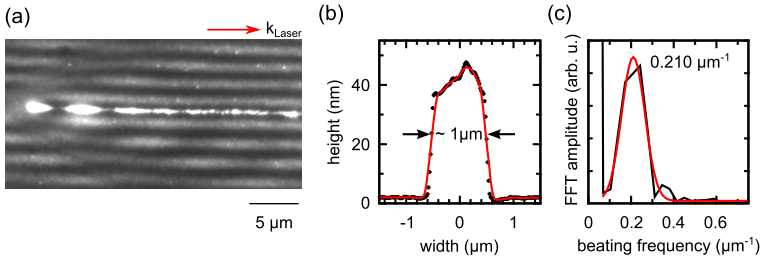

Fig. 5. (a) Two-photon PEEM image of a p-6P nanofiber prepared in another deposition run showing a considerably deviating cross section in comparison to the nanofibers of the sample shown in Fig. 1; (b) AFM cross section of the nanofiber in (a); (c) FFT spectrum of the two-photon PEEM beating pattern; the DLSPPW shows a beating period of 4.76 µm, corresponding to a SPP wavelength of 745 nm.

Knowledge of the SPP group velocity enables us to finally perform a fit to the intensity profile of the static PEEM measurements (see Fig. 2(c)) with the damping length κ and the ratio A in the electric field amplitude between laser pulse and SPP wave packet as the only free parameters. The result of the fit is added as a red line to Fig. 2(c). The best fit yields a propagation constant $\kappa = 39$ µm and a value $A = 0.59$. The value for κ is particularly consistent with the decay length of the beating pattern of 15 µm, which is additionally reduced by the group velocity mismatch between laser pulse and SPP.

In Fig. 5(a) we finally show static 2P-PEEM measurements of a p-6P nanofiber grown under different preparation parameters and deposited onto another gold substrate, this time by means of the stamping transfer technique. At a nanofiber height of about 45 nm the resulting SPP waveguide has a width of 1 µm (see Fig. 5(b)) and is therefore significantly broader than the waveguides of the first sample. The PEEM data give clear evidence that the modified waveguiding geometry also affects the waveguiding properties. The FFT spectrum of the nanofiber intensity profile shown in Fig. 5(c) provides a beating pattern periodicity of 4.76 µm, corre-

#182243 - $15.00 USD Received 21 Dec 2012; revised 14 Feb 2013; accepted 14 Feb 2013; published 28 Mar 2013

sponding to a SPP wavelength of 745 nm ($n_{\mathrm{eff}} = 1.074$). A trend to larger effective index of refraction for increasing width of the waveguide is indeed expected from effective index theory [13].

4. Conclusions

Para-hexaphenylene nanofibers exhibit a variety of interesting optical properties which makes them highly attractive for the use in nanooptical devices. In this work we particularly addressed the capability of deposited p-6P nanofibers to act as dielectric loaded SPP waveguides. In a combined static and time-resolved PEEM experiment we were able to determine for a specific nanofiber geometry the relevant SPP propagation parameters, namely phase velocity, group velocity and damping length. Furthermore and in qualitative agreement with theoretical predictions, we could experimentally show that the SPP propagation is considerably affected by the details of the fiber geometry. The high degree of flexibility in designing p-6P based nanofibers of different dimensions and different cross-sectional shape [41], hence opens up the possibility to fabricate custom-made SPP waveguides for designated applications. For instance, the SPP damping length, one of the most critical parameters for the use in plasmonic circuits, is predicted to significantly depend on the height of the nanofibers [13]. This perspective asks for ongoing systematic studies on SPP waveguiding in this type of nanooptical building block.

Acknowledgments

This work was funded by the German Science Foundation (DFG) through Priority Program 1391 ”Ultrafast Nanooptics” as well as by the Danish Research Agency through various grants.

#182243 - $15.00 USD Received 21 Dec 2012; revised 14 Feb 2013; accepted 14 Feb 2013; published 28 Mar 2013